Duplicated genes with split functions: independent roles of *protocadherin15* orthologues in zebrafish hearing and vision

Christoph Seiler[1], Karin C. Finger-Baier[1], Oliver Rinner[2], Yuri V. Makhankov[2], Heinz Schwarz[1], Stephan C. F. Neuhauss[2] and Teresa Nicolson[3,*]

[1]Max Planck Institut fur Entwicklungsbiologie, Spemannstrasse 35, 72076 Tübingen, Germany
[2]Brain Research Institute, University of Zurich and Department of Biology, Swiss Federal Institute of Technology Zurich, Winterthurerstr. 190 8057 Zurich, Switzerland
[3]Oregon Hearing Research Center and Vollum Institute, Oregon Health and Science University, 3181 SW Sam Jackson Park Road, Portland, OR 97239, USA
*Author for correspondence (e-mail: nicolson@ohsu.edu)

Accepted 23 November 2004

Development 132, 615-623
Published by The Company of Biologists 2005
doi:10.1242/dev.01591

Summary

In the sensory receptors of both the eye and the ear, specialized apical structures have evolved to detect environmental stimuli such as light and sound. Despite the morphological divergence of these specialized structures and differing transduction mechanisms, the receptors appear to rely in part on a shared group of genes for function. For example, mutations in Usher (USH) genes cause a syndrome of visual and acoustic-vestibular deficits in humans. Several of the affected genes have been identified, including the *USH1F* gene, which encodes protocadherin 15 (PCDH15). *Pcdh15* mutant mice also have both auditory and vestibular defects, although visual defects are not evident. Here we show that zebrafish have two closely related *pcdh15* genes that are required for receptor-cell function and morphology in the eye or ear. Mutations in *pcdh15a* cause deafness and vestibular dysfunction, presumably because hair bundles of inner-ear receptors are splayed. Vision, however, is not affected in *pcdh15a* mutants. By contrast, reduction of *pcdh15b* activity using antisense morpholino oligonucleotides causes a visual defect. Optokinetic and electroretinogram responses are reduced in *pcdh15b* morpholino-injected larvae. In electron micrographs, morphant photoreceptor outer segments are improperly arranged, positioned perpendicular to the retinal pigment epithelium and are clumped together. Our results suggest that both cadherins act within their respective transduction organelles: Pcdh15a is necessary for integrity of the stereociliary bundle, whereas Pcdh15b is required for alignment and interdigitation of photoreceptor outer segments with the pigment epithelium. We conclude that after a duplication of *pcdh15*, one gene retained an essential function in the ear and the other in the eye.

Key words: Protocadherin 15, Hair cell, Photoreceptor, Zebrafish, Deafness, Blindness, Outer segment, Stereocilia, Gene duplication, *orbiter*

Introduction

Sensory receptors in the ear and eye are thought to have evolved from a common ancestral ciliated cell (reviewed by Popper et al., 1992). Both receptors have highly specialized apical surfaces. Receptor cells in the ear possess an apical bundle of actin-filled stereocilia that transduce mechanical stimuli (reviewed by Hudspeth, 1989), whereas the photoreceptors of the eye have an outer segment that contains membrane disks specialized for detection of light. Through genetic studies, several molecules required for both hearing and vision have been identified. In humans, mutations in these genes cause Usher syndrome (for a review, see Petit, 2001), one of the most prevalent inherited disorders (Ahmed et al., 2003b). Individuals suffering from Usher 1 syndrome are born deaf and develop visual problems in the second to fourth decade of life due to retinitis pigmentosa. Mutations in most of these genes have been shown to cause deafness in mice as well, but no phenotype comparable to retinitis pigmentosa has been reported (reviewed by Steel and Kros, 2001; Ball et al., 2003; Libby et al., 2003).

As in mammals, fish sense mechanical stimuli with hair cell receptors in the inner ear and an additional sensory system unique to aquatic animals, the lateral line (Manley and Koppl, 1998; Popper and Fay, 1997). In recent screens for genes necessary for inner ear function in zebrafish larvae, 24 loci linked to an auditory/vestibular-specific phenotype were identified (Nicolson et al., 1998) (T.N., unpublished). Here we show that the zebrafish auditory/vestibular mutant *orbiter* is affected in the gene *pcdh15*. Mutations in *PCDH15* have been recently shown to be the cause of human Usher syndrome 1F (Ahmed et al., 2001; Alagramam et al., 2001b; Ben-Yosef et al., 2003) and deafness in Ames waltzer mice (Alagramam et al., 2001a). Furthermore, we report the characterization of a second, duplicated *pcdh15* gene in zebrafish, which is expressed in the retina. Our results indicate that one gene acquired an essential function in the

eye and the other one in the ear. Both genes are required for the structural integrity of the respective receptor cells in these organs.

Materials and methods

Zebrafish strains

All studies were done with larvae in the Tübingen (Tü) background. *albino* larvae were used for in situ hybridization. Zebrafish stocks were maintained as described (Haffter et al., 1996).

Mapping and cloning

Linkage analysis was performed using WIK wild-type fish crossed with heterozygous *orbiter*^{th263b}-Tü fish. The mutation was mapped using SSLP (simple sequence length polymorphisms) and SSCP (single strand conformation polymorphisms) (Cleangels SSCPplus gels were used according to the manufacturer's instruction; ETC, Kirchentellinsfurt, Germany). For fine-mapping, single mutant larvae were tested for recombination events. To initiate a chromosomal walk, we used the marker z26404 to screen PCR-able pools of genomic zebrafish BAC (BioCat, Heidelberg, Germany) or PAC (RZPD, Berlin, Germany) libraries. All clones found were sized using pulsefield gel electrophoresis. New SSLP or SSCP markers were created using sequences from the ends of the identified BAC- or PAC-clones. After defining a critical interval, six clones spanning the contig (PAC1, BAC1, PAC10, PAC13, BAC6, BAC7) were sequenced at the Sanger Center (Welcome Trust Sanger Institute, Cambridge, UK). The sequence within the critical interval was analyzed using Genscan (http://genes.mit.edu/GENSCAN.html) and blast searches of the NCBI database (http://www.ncbi.nlm.nih.gov/BLAST).

To clone the 3′ and 5′ ends of the genes several rounds of RACE with either the Marathon or SMART RACE cDNA amplification kit (Clontech, Palo Alto, CA) were performed according to the manufacturers' instruction. The Goodfellow T51 panel was used to map *pcdh15b* (Geisler et al., 1999). Mapping prediction on the T51 panel map was done using the 'Instant Mapping' website from The Children's Hospital Zebrafish Genome Project Initiatives (http://zfrhmaps.tch.harvard.edu/ZonRHmapper/instantMapping.html).

GenBank accession numbers and clone names

The official names of the PAC clones from RZPD are the following: PAC1: BUSMP706C1835Q2; PAC5/7: BUSMP706H0192Q2; PAC9: BUSMP706M01204Q2; PAC12: BUSMP706N24105Q2; PAC10: BUSMP706N24105Q2; PAC11: BUSMP706O192Q2; PAC13: BUSMP706J031239. See the RZPD-Database (https://www.rzpd.de) for further information. GenBank accession number of the clones sequenced by the Sanger center: BAC1: AL592289; BAC6: AL592062; BAC7: AL645689; PAC10: AL592202; PAC13: AL592204; PAC1: AL592077. GenBank accession numbers for zebrafish *pcdh15a*: AY772390; and *pcdh15b*: AY772391.

Mutation analyses

Total RNA was prepared from pools of 5-10 wild-type sibling or mutant larvae using the NucleoSpin RNAII Kit (MACHEREY-NAGEL, Easton, PA). Reverse transcription reactions were performed using the Superscript reverse transcriptase (Invitrogen, Carlsbad, CA) with an oligo (dT) primer.

In situ hybridization

Whole mount in situ hybridization was performed as described (Schulte-Merker et al., 1994). A fragment containing bp 180-1800 from the extracellular domain (Fig. 2) or bp 4516-5908 from the polymorphic intracellular part were used as probes for *pcdh15a*. Both probes gave the same signal; the signal with the extracellular probe was stronger and appeared more specific. bp 4075-5697 from the intracellular part was used as probe for *pcdh15b*.

Cryosectioning

For cryosectioning, larvae were immersed with increasing concentration of fish gelatin (FG, 8-25%) (Sigma G-7765 or G-7041) and sucrose (SC 8-15%) in Ringers during a 48-hour period at room temperature. They were transferred to forms made of aluminium foil covered with 20% FG, 15% SC and quickly frozen on a metal plate bathing in liquid nitrogen. 14 μm sections were cut at –20°C using a Leica CM 3050 cryomicrotome.

Electron microscopy

For electron microscopy, larvae were processed as previously described (Seiler and Nicolson, 1999). Whole larvae were embedded in Epon and oriented such that the eye was sectioned in a transverse dorsal to ventral direction. All sections were done in the plane of the optic nerve. Images were taken from areas adjacent to the optic nerve in the center of the retina.

Morpholino injections

Four different morpholinos were used in this study and injected at the one cell stage as described (Nasevicius and Ekker, 2000). One was directed against the translation start (ATG Mo) of *pcdh15b* with the sequence 5′-CCACGACCTCTGGCGATCTTCATA-3′, one against the 3′ splice site of coding exon number 4 (GT Mo) with the sequence 5′-AAAAGATAATCACATCTCGGTCCAG-3′, and an unrelated control morpholino (a 4 bp mismatched oligo against *fkd6;* 5′-CGACGAGCTCTGCCGATCTTGATA-3′). A second control morpholino was a 4 bp mismatched oligo against *pcdh15b* (5′-TGCGCGCCAGACAGGGTGATGAC-3′). In the ATG Mo-injected larvae (40 ng), a slightly shorter body axis of the larvae was occasionally observed. Differentiation of other organs like the heart, brain and ear appeared normal, indicating that this effect was not due to a delay in development. To ensure that the 40 ng dose had no effect on the onset of eye differentiation, we stained 14 μm sections of eyes of these larvae with anti-tyrosine hydroxylase antibody and counted the positive cells. No difference in number could be detected between uninjected (1.4 cells/section n=13) and larvae injected with 40 ng ATG Mo (1.5 cells/section n=14).

Fluorescent staining and microscopy

For confocal microscopy, an inversed Leica DM IRBE microscope equipped with a 100× oil lens was used. For antibody staining, the larvae were fixed with 4% formaldehyde in PBS for at least 24 hours prior to sectioning. The sections were incubated with 1% bovine serum albumin. The following antibodies were used in this study: *zpr-1* (The zebrafish international resource Center, Eugene, OR, USA), *rhod-1* (Ret-P1, Milan, Analytica AG/Switzerland), and Alexa488 goat anti-rabbit Ab (Molecular Probes, Eugene, OR).

Optokinetic stimulation

Single larvae were placed dorsal side up in the center of a petridish (35 mm diameter) containing 3% prewarmed (28°C) methylcellulose. Moving gratings were projected by a Proxima 4200 DLP projector onto a screen within the visual field of the larva, at an apparent distance 4.65 cm from the larva's right eye. Projection size on the screen was 8 cm × 6 cm, subtending a visual angle of 65.6° horizontally and 53.1° vertically. A custom-made graphics library running under Microsoft DOS, allowing full control of timing and intensity of the projection was used to create the stimuli. Mean intensity levels were adjusted by introducing neutral density filters into the light beam. The contrast C of grating stimuli was calculated from: $C = (I_{max} - I_{min})/(I_{max} + I_{min})$.

Spatial frequency of the grating stimulus was varied between 0.025 and 0.14 cycles/°. All measurements were made under a mean

luminance of 120 cd/m^2, temporal frequency of 0.4 Hz, pattern contrast of 62.5% and a grating velocity of 7.6°/second.

We measured the CSF in 4-day-old larvae injected with either an ATG Mo (40 ng *n*=7 or 30 ng *n*=7) or the control Morpholino (40 ng *n*=7). The experiment has been repeated with similar results in an independently injected clutch.

ERG recordings

Electroretinograms (ERGs) were performed on larvae at 4.5 dpf as previously described (Makhankov et al., 2004). All pre-recording steps were done under red illumination to minimize bleaching of the visual pigment. Preparation and recordings were performed in a tight Faraday cage. All specimens were dark-adapted for 30 minutes prior to positioning them in the recording chamber. Each larva was placed on its side on the surface of a moist sponge with E3 medium (mM: 5 NaCl, 0.17 KCl, 0.33 $CaCl_2$ and 0.33 $MgSO_4$) and paralyzed by directly adding a droplet of the muscle relaxant Esmeron (0.8 mg/ml in larval medium; Organon Teknika, Eppelheim, Germany). The Ag/AgCl electrode system was used to record the ERG response. The recording electrode was positioned in the center of the cornea. The reference Ag/AgCl pellet was placed under the body of the larva. A 3-minute period was chosen to adapt the larvae to both dark- and light-adapted states prior to measurement. Relative background light intensitiy was 175 lux for the light-adapted state. The duration of light stimulus was 100 mseconds with an interstimulus interval of 5 seconds. Stimulus illumination was increased in 0.5 log unit steps over the range from –5 log unit to –1 log unit. Unattenuated light intensity over the subject's head was 20,000 lux (optical density, OD was equal 0 log unit), as measured by a light meter (Tekronix J17, Texas Instruments, USA). A virtual instrument (VI) under NI LabVIEW 5.1 was developed to use in all experiments. Amplified analog signals were sampled by means of NI PCI 6035E DAQ board connected to a NI BNC-2090 BNC terminal block. Sampling was done in buffered acquisition mode with a sampling rate of 250 Hz. Recording was triggered by the shutter signal. To analyze the ERG response with respect to the actual onset of the light stimulus, mechanical shutter delay was measured by means of a photodiode. Traces were normalized to the baseline by subtracting the average potential before the stimulus onset. Responses were averaged between three and five, times depending on the signal-to-noise ratio.

Results

The *orbiter* gene encodes Protocadherin 15

Mutant *orbiter* zebrafish larvae have a vestibular defect and cannot sense acoustic-vibrational stimuli (Granato et al., 1996; Nicolson et al., 1998). Extracellular microphonic potentials of *orbiter*^{th263b} mechanosensory hair cells are absent, suggesting that the primary events in the mechanotransduction process are affected (Nicolson et al., 1998). To identify the *orbiter* gene, we undertook a positional cloning approach. By testing 2951 mutant larvae for recombination events using polymorphic CA repeat markers, we mapped *orbiter* to chromosome 13, north of the marker z26404 (4 recombinations in 2951 larvae) and south of the marker z25253 (99 recombinations in 2780 larvae). Using z26404, we started a chromosomal walk and constructed a contig comprising several BAC and PAC clones that spanned the critical interval (Fig. 1A). To identify the affected gene, three PAC and three BAC contig clones were sequenced. Analysis of these sequences revealed that these clones contain exons present in the first half of a gene that is homologous to human and mouse protocadherin 15 (*PCDH15*). The entire contig contained bp 1-3225 of *pcdh15*; bp 1352-3225 was within the critical interval. No other genes were present on the clones. We performed RACE to clone the full-length zebrafish *pcdh15* gene, which we designated *pcdh15a* (see below). Sequence analysis revealed that it shares high homology with human and mouse protocadherin 15. The Pcdh15 protein belongs to a class of atypical cadherins: the protein is composed of 11 cadherin repeats, a single transmembrane domain, and an intracellular domain with no similarity to other proteins (Fig. 1B).

The five *orbiter* alleles can be grouped in two phenotypic classes. One class causes strong defects such as no response to acoustic vibrational stimuli and a vestibular defect, no uptake of the styryl dye FM1-43 into hair cells, and no detectable microphonic potentials [microphonics only measured in *th263b* (Nicolson et al., 1998)]. This class includes the *th263b*,

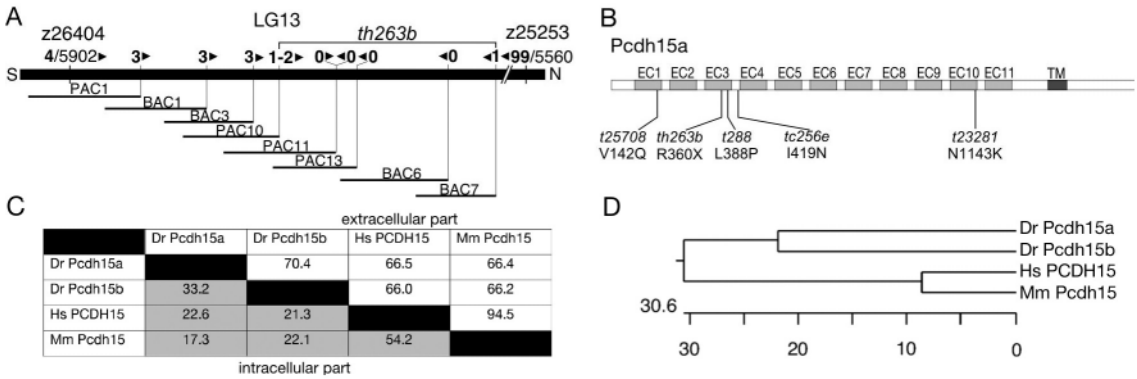

	Dr Pcdh15a	Dr Pcdh15b	Hs PCDH15	Mm Pcdh15
Dr Pcdh15a		70.4	66.5	66.4
Dr Pcdh15b	33.2		66.0	66.2
Hs PCDH15	22.6	21.3		94.5
Mm Pcdh15	17.3	22.1	54.2	

Fig. 1. Zebrafish have two *pcdh15* genes. (A) Cloning of *pcdh15a*. The *orbiter*^{th236b} locus maps to chromosome (LG) 13 between the simple sequence length polymorphic (SSLP) markers z26404 and z25253. The critical interval was determined by generating SSLP markers from overlapping BAC and PAC clones and testing for recombination events in larvae identified with the south marker z26404 (indicated by arrowheads pointing to the right) or north marker z25253 (arrowheads to the left). Sequencing of six clones spanning the contig identified exons of the gene *pcdh15a*. No other gene was present. (B) Schematic diagram of the Pcdh15a protein. The mutations identified in *orbiter* are indicated below. (C) Comparison of the predicted extracellular and intracellular domains of zebrafish Pcdh15a and Pcdh15b with the human and mouse PCDH15 proteins. Similarity of the extracellular regions is in the upper right half of the table; the intracellular regions are in the lower left half, shaded in grey. Extracellular domains of human, mouse, and zebrafish Pcdh15 are more conserved than the intracellular domain. (D) Phylogeny of human, mouse, and zebrafish Pcdh15 proteins are shown. The scale indicates phylogenetic distance by substitution events.

t25708, and *t288* alleles. The other class is a weak, hypomorphic class with occasional response to acoustic vibrational stimuli but a fully penetrant vestibular defect, weak uptake of FM1-43 (data not shown) (Nicolson et al., 1998; Seiler and Nicolson, 1999), and reduced microphonic potentials [*tc256e* (Nicolson et al., 1998)]. The weaker alleles include *tc256e* and *t23281*.

Sequencing of *pcdh15a* cDNA from the mutants revealed that it is the gene affected in *orbiter* mutants. For the alleles of the strong class, we found that the mutation in *t25708* leads to a valine to glutamine exchange (V142Q) in close proximity to the conserved cadherin calcium-binding motif (with the consensus DXNDN) of the first cadherin domain. The mutation in *th263b* causes a truncation of the protein in the third cadherin repeat (R360X), presumably resulting in a nonfunctional protein. *t288* causes a leucine to proline (L386P) exchange, adjacent to the calcium binding domain of the third cadherin domain (here DENNQ instead of DXNDN) (Fig. 1B).

Sequencing of the alleles of the hypomorphic class revealed that *tc256e* causes an isoleucine to asparagine (I419N) exchange in the linker between the third and fourth cadherin domain. *t23281* causes an asparagine to lysine (N1143K) exchange in the tenth cadherin domain, changing the calcium-binding motive from DENDH to DEKDH (Fig. 1B). The weaker phenotype seen in homozygous *t23281* animals suggests that this cadherin domain is less critical for Pcdh15 function.

A second zebrafish *pcdh15* gene

In addition to the *pcdh15* gene mutated in *orbiter,* we identified a second ortholog of *pcdh15*. We designated the gene mutated in *orbiter* as *pcdh15a,* and the other gene *pcdh15b*. *pcdh15b* is located on chromosome 12 between the markers *dkk1* and z1473 (T51 RH panel). The predicted Pcdh15b protein has the same domain structure and shares high amino acid similarity (70%) with the extracellular domain of zebrafish Pcdh15a, and mouse and human PCDH15 (Fig. 1C). The intracellular domain is less similar to the intracellular domains of Pcdh15a and mouse and human protocadherin 15 (17-33%, Fig. 1C), but the intracellular tail is divergent among all species (Fig. 1C). Nevertheless, all Pcdh15 intracellular domains share the feature of being proline- and serine-rich, and there are short stretches of high similarity. Pcdh15b has a putative PDZ class I binding motif at its C-terminus [consensus X-S/T-X-L (Sheng and Sala, 2001)]. This motif is also conserved in human and mouse PCDH15, but is not present in zebrafish Pcdh15a, which is shorter at the C-terminus.

Phylogenetic analysis based on a ClustalW alignment revealed that the two zebrafish proteins are more related to each other than to the mammalian orthologs (Fig. 1D). This suggests that they were duplicated after the split of the mammalian and fish lineage, probably during the suggested genome duplication event in ray-finned fish (Prince and Pickett, 2002; Taylor et al., 2003).

Expression of *pcdh15a* and *pcdh15b* in the ear and the eye

To determine the spatial and temporal expression of *pcdh15a* and *pcdh15b,* we performed mRNA *in situ* hybridization. At the four-somite stage (11 hours post fertilization, hpf), *pcdh15a* is expressed in the anterior neuroectoderm and in the first forming somites (Fig. 2A). At 24 hpf, *pcdh15a* is expressed in the eye (Fig. 2B) and hatching gland (out of focus). Expression is also detectable in the newly developed mechanosensory hair cells (Fig. 2B,C). Expression of *pcdh15a* in hair cells was visible in all later stages investigated (Fig. 2D-F′). At day 3, additional expression in regions of the brain is present, together with expression at the lateral borders of the epiphysis (Fig. 2D). At day 4, expression in the brain persists and is detectable in the hair cells of neuromasts (Fig. 2E,F′). Within the neuroepithelia of the ear and lateral line, levels of *pcdh15a* mRNA are highest in the hair cells (Fig. 2F,F′).

pcdh15b is weakly expressed in the whole embryo at 24 hpf (data not shown). At 48 hpf, strong expression in the epiphysis is visible but not in the eye (data not shown). At day 2.5, the gene is expressed at the ventral margin of the eye (Fig. 3A), where the first photoreceptors differentiate. Following the wave of differentiation of photoreceptors (Larison and Bremiller, 1990; Raymond et al., 1995), *pcdh15b* is expressed in the proximal regions of the eye around day 3 and restricted to the lateral margin at day 5 (Fig. 3B,C). In thick sections, expression is evident in photoreceptors (Fig. 3E,F). In addition, *pcdh15b* is expressed in the brain and center of the epiphysis at day 3 (Fig. 3D) and 5. Weak expression was detected in the

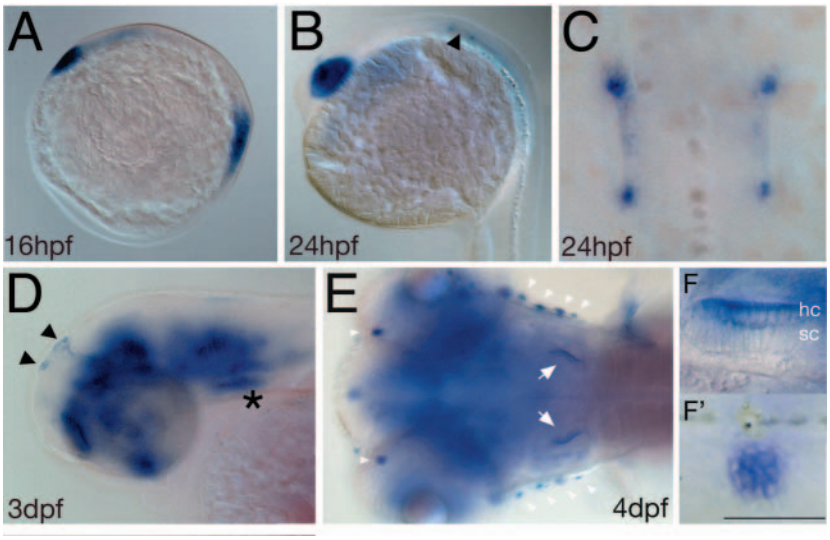

Fig. 2. Expression pattern of *pcdh15a* using in situ hybridization. (A-E) *pcdh15a* expression in embryos and larvae. At the four-somite stage (A), *pcdh15a* is expressed in the anterior neuroectoderm and in the somites. At 24 hpf (B), there is expression in the eye, the hatching gland (blue shading under the eye, out of focus) and the first hair cells of the ear at the margins of the otic vesicle (arrowhead and panel C). At 3 dpf (D), expression of *pcdh15a* is not detectable in the eye, whereas expression is present in the ear (asterisk), the brain and the lateral parts of the epiphysis (arrowheads). At 4 dpf (E), expression is present in the hair cells of the ear (arrows indicate the posterior maculae present in this focal plane) and the neuromasts (arrowheads). (F) Higher magnification view of the *pcdh15a*-positive hair cells of the anterior macula. (F′) Higher magnication view of a trunk neuromast. Scale bar in F′: 180 μm for A,B; 50 μm for C; 120 μm for D; 150 μm for E; 30 μm for F; 20 μm for F′.

ear and neuromasts (data not shown). No signal was detected with the corresponding sense probes.

orbiter/pcdh15a is required for hair-bundle integrity

To analyze the hair bundles in *orbiter* mutants in more detail, we stained the actin-filled stereocilia of the hair bundles with fluorescently-labeled phalloidin (Fig. 4). We observed a moderate degree of splaying in the hair bundles in the semicircular canals in the strong allele *th263b* (Fig. 4B). Not all stereocilia were split apart, and some bundles appeared normal. Hair bundles were less affected in larvae carrying the weak allele *tc256e* (Fig. 4C). The defect in *th263b* is much weaker in comparison to other splayed-bundle mutants like *mariner* (Fig. 4D).

In Ames waltzer/*Pcdh15* mutant mice, the planar polarity of the hair bundle of cochlear hair cells was sporadically disturbed, with hair cells rotated at 90° (Alagramam et al., 2001a; Raphael et al., 2001). By staining the actin in the bundle and the cuticular plate with fluorescently-labeled phalloidin, we could visualize the polarity of the hair bundles in zebrafish neuromasts (NM), because the kinocilium and its insertion point are not stained with phalloidin. The kinocilium is located at either the caudal or rostal margin of the hair cell (n=12 NM, three specimens) (Fig. 4E-F). No difference in polarity could be detected in *th263b* (n=10 NM, 5 spec) (Fig. 4E′-F′; arrows indicate orientation each bundle with arrowhead pointed towards the kinocilium; see Fig. S1 in the supplementary material for more examples). The number of hair cells (HC) in neuromasts was reduced (12.5 HC/NM in *tc263b*; 17HC/NM in WT; counting NM above and around the ear) (Fig. 4F). A similar reduction was seen in *mariner* neuromasts (13,25 HC/NM, n=12, 3 spec). It is not clear why the hair bundles in Ames waltzer mice have a polarity defect, whereas mutant *orbiter* hair bundles do not.

pcdh15b morphants have reduced contrast sensitivity and retinal function

To determine the function of Pcdh15b, we designed two morpholinos: one against the ATG translational start site (ATG Mo), and one against the GT splice site of the fourth coding exon (GT Mo). The ATG Mo is predicted to inhibit the initiation of translation of *pcdh15b* message, whereas the GT Mo should prevent the correct splicing of exon 4. Because the ATG Mo inhibits protein synthesis of Pcdh15b, its efficiency cannot be evaluated at the mRNA expression level. However, we could test the efficiency of the GT Mo by amplifying cDNA with primers flanking the targeted exon. RT-PCR analysis confirmed that the GT Mo indeed caused aberrant splicing of the targeted exon. Wild-type transcript levels are reduced by approximately 60% on day 3, and reduced by 40% on day 4 (Fig. 5D). The results of the histological analysis and electroretinograms (see below) suggest that the ATG Mo was more effective than the GT Mo. Morpholino-injected animals appeared to develop normally and overall morphology was normal (see Fig. S2 in the supplementary material). No obvious defects in balance or the acoustic startle reflex or hair bundle morphology were observed in *pcdh15b* morpholino-injected (morphant) larvae (data not shown). In addition, we examined uptake of the vital dye, FM1-43, an indicator of mechanotransduction in zebrafish hair cells (Seiler et al., 1999). Uptake was unaffected in *pcdh15b* morphants (see Fig. S3 in the supplementary material).

To test whether morphant larvae have a visual defect, we measured the optokinetic response (OKR). The OKR is a reflexive movement of the eye when stimulated with a moving pattern. The velocity of the eye movement depends on the density and contrast of the pattern. We measured the gain (eye velocity/stimulus velocity) of 4-day-old larvae injected with 40 ng of an unrelated control morpholino (control Mo) and larvae injected with 30 ng or 40 ng ATG Mo during stimulation with increasing spatial frequency (i.e. decreasing stripe width of the moving grate) (Fig. 5A). Comparison of the *pcdh15b* morphants with control injected larvae (40 ng, n=7) revealed a significant difference in sensitivity (ANOVA with repeated measures, d.f.=2, F=44.1, a<0.001). The comparison of responses in larvae injected with 40 ng or 30 ng *pcdh15b* ATG Mo is significant as well (a<0.001), indicating an obvious dosage effect. The experiment was repeated, obtaining similar results in an independently injected clutch of eggs (data not shown, n=7, 40 ng ATG Mo, 31% reduction in contrast sensitivity). In contrast, no OKR defect was detectable in *orbiter*^{th263b} mutant larvae when compared to wild-type larvae (data not shown).

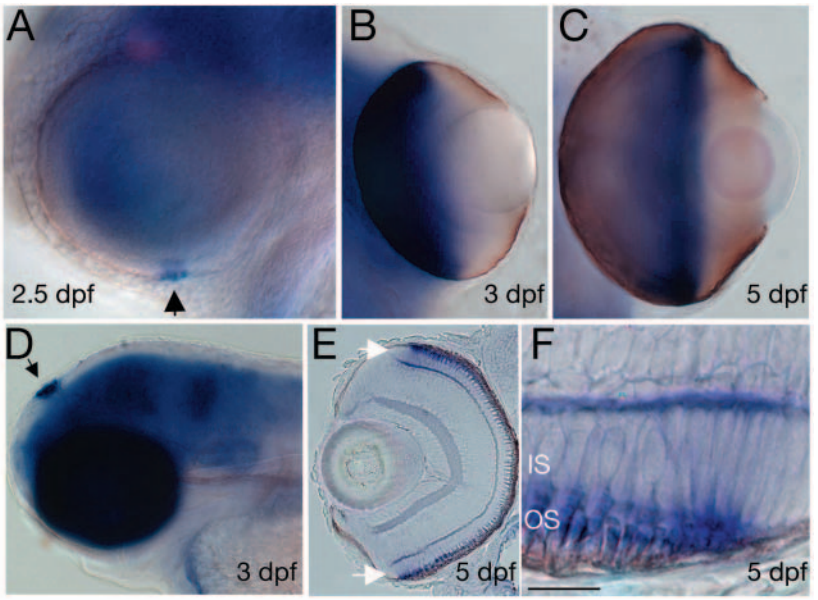

Fig. 3. Temporal expression pattern of *pcdh15b* in differentiating photoreceptor cells. (A) At 2.5 dpf, *pcdh15b* is expressed in the first differentiating photoreceptors at the ventral margin of the eye (arrowhead). (B) At 3 dpf, the whole proximal optic cup is stained. (C) At 5 dpf, expression is only present at the margin of the optic cup, no expression is visible in the proximal eye. (D) Expression in the epiphysis (arrow) and brain at 3 dpf. *pcdh15b* expression in the eye is specific to photoreceptor cells (E,F; cryosection of a larva stained as in C) Arrows in (E) indicate photoreceptor proliferation zones shown at higher magnification in (F). Scale bar in F, 50 μm for A; 40 μm for B,C,E; 150 μm for D; and 5 μm for F. IS, inner segment; OS, outer segment.

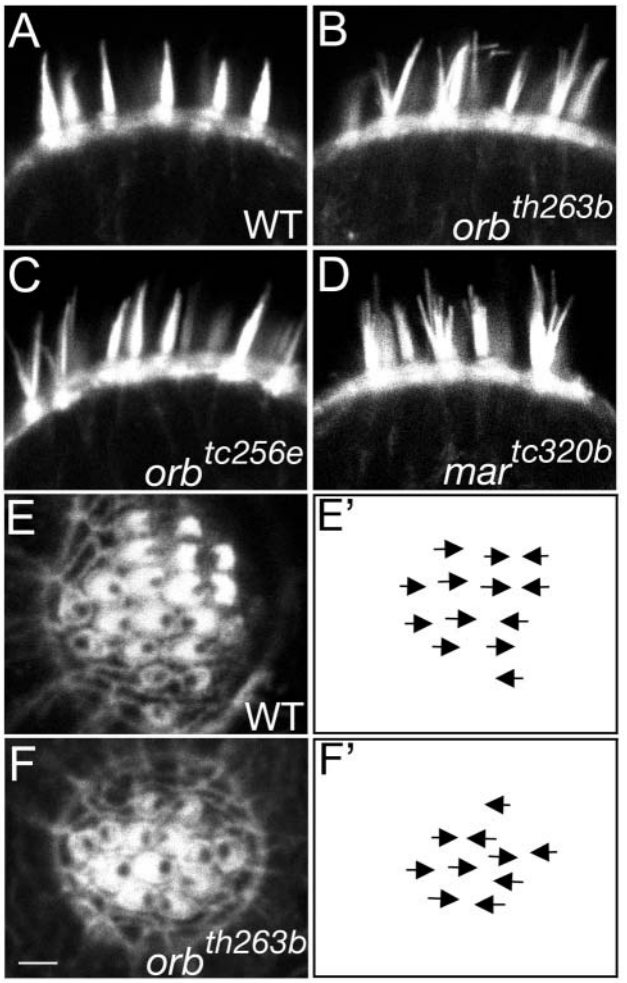

Fig. 4. *orbiter* mutants have a splayed hair-bundle phenotype. (A-D) The actin of the mechanosensory hair bundles of the lateral cristae were labeled with Alexa488-Phalloidin, and visualized in transverse sections with a confocal microscope. In wild-type larvae (A), the bundles are conical and intact in comparison to bundles in *orbiter*^{th263b} (B). A similar phenotype is visible *tc256e* bundles (C), but many intact bundles are still present. A null allele of *mariner/myosin VIIA* (D) causes a more severe phenotype than *th263b* (B). (E,F) Horizontal optical sections of lateral line hair bundles. The unstained insertion point of the kinocilium is located at the caudal or rostral margin of the hair cells. No differences in planar polarity were observed between wild-type or *th263b* bundles as indicated with arrows (pointed toward each kinocilium) in (E′) and (F′). Scale bar: 1 μm.

To determine whether injection of *pcdh15b* morpholinos results in physiological defects that are specific for retinal function, the electroretinogram (ERG) b-wave was measured in 4.5-day-old larvae. Larvae injected with 40 ng of the ATG Mo (n=6) or 16 ng of the GT Mo (n=6) were compared with uninjected larvae (n=5) and larvae injected with the control Mo (n=5). As shown in Fig. 5B and C, the b-wave increases in amplitude with increasing stimulus intensity in all experimental groups. Injection of both morpholinos resulted in a significant reduction in b-wave amplitude. (3-way ANOVA d.f.=3, F=11.7, a<0.001). Although both morpholinos are targeted against different sequences, they cause a comparable reduction in b-wave amplitude, indicating that this effect is specific for the knockdown. Comparison of the *pcdh15b* morphants with control-injected and uninjected larvae is significant for 40 ng ATG MO (a<0.001) and 16 ng GT MO (a<0.001; Scheffe test). The weaker b-wave amplitude reduction between the GT Mo compared to the ATG Mo injected larvae was not significant, though. Representative traces from individual specimens are shown in Fig. 5E,F. Due to a very low amplitude and differing width, we were not able to evaluate the a-wave data conclusively. Nevertheless, our behavioral and physiological analyses indicate a clear defect in retinal responses in *pcdh15b* morphants.

Reduction of *pcdh15b* activity affects photoreceptor morphology

To determine if the visual defect is due to a morphological defect in the retina, we examined cryosections of morpholino-injected larvae using immunohistochemistry. In larvae injected with 30 ng (n=5) or 40 ng (n=7, 2 independent experiments) of the ATG Mo, we observed a dose-dependent phenotype in the retinal photoreceptor cell layer (Fig. 6). The *zpr-1* antibody labels double cone photoreceptor cell bodies and outer segments (Larison and Bremiller, 1990). In 4-day old morphants, the general morphology of the photoreceptors labeled with *zpr-1* antibody appeared disorganized. Labeled cells appeared wider, shorter, and deformed (Fig. 6A-F). Effects were also evident using an anti-rhodopsin (*rhod-1*) antibody that labels outer segments. Outer segments of the rod photoreceptors appeared shorter and less organized than wild-type outer segments (Fig. 6G-I). The effects on both rods and cones seen with the antibodies were stronger in larvae injected with 40 ng (Fig. 6F,I) than in larvae injected with 30 ng ATG Mo (Fig. 6E,H).

To examine the morphological defect at the ultrastructural level, we performed transmission electron microscopy (TEM) with thin sections of 4-day-old larvae. We compared uninjected (n=2) larvae to larvae injected with either 40 ng ATG Mo (n=3), 16 ng GT Mo (n=2) or 40 ng control (n=2) or 4 bp mismatch (n=3) control Mo. In the ATG Mo-injected larvae, the layer of photoreceptor nuclei appeared more compacted than in uninjected larvae (Fig. 7A,B). The outer segments of the photoreceptors were often tilted sideways and clustered together. In addition, the number of pigment cell granules positioned between the outer segments was greatly reduced (Fig. 7C). This effect was still present in 7-day-old larvae, though the outer segments were more clustered and less tilted (Fig. 7E,F). A similar but weaker defect was visible in the GT Mo-injected larvae (data not shown). A lack of interdigitation of the outer segments and therefore the absence of the protective ensheathing by the pigmented epithelium is consistent with the poorer performance of the *pcdh15b* morphants under bright-adapting conditions. Defects were not detectable in the control Mo-injected larvae or in larvae injected with a *pcdh15b* 4 bp mismatch morpholino (Fig. 1A′). In addition, we also examined *orbiter*^{th263b} retinas using TEM, and did not observe any obvious defects (data not shown).

Discussion

Here we show that *protocadherin 15*, responsible for retinitis pigmentosa and congenital deafness in humans (Ahmed et al.,

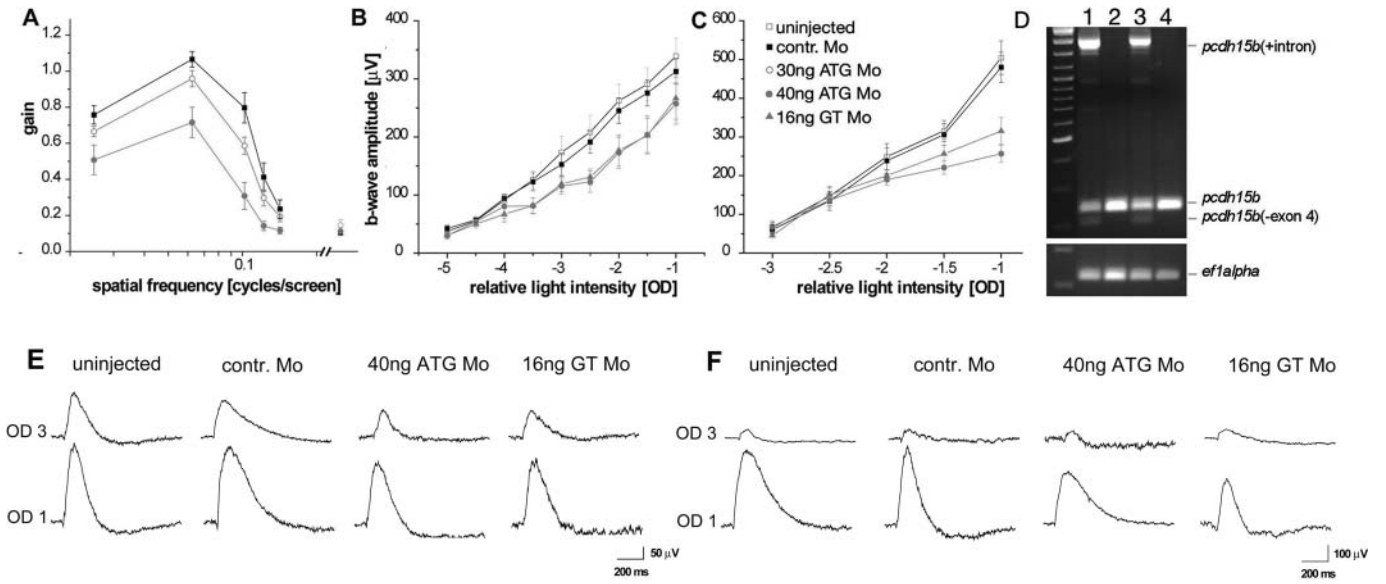

Fig. 5. Behavioral analysis and ERG recordings of *pcdh15b* morphants. (A) Optokinetic responses were measured as a function of spatial frequency of a moving square pattern. Larvae injected with 40 ng ATG Mo (filled circles) have reduced contrast sensitivity and visual acuity compared with control injected larvae (filled squares). Larvae injected with 30 ng ATG Mo (open circles) show a slightly reduced visual performance. (B) *pcdh15b* knock-down results in significantly reduced retinal sensitivity to light under dark- and light-adapting states. The ERG b-wave amplitudes in the dark-adapted (B) and light-adapted state (C) are plotted as a function of relative light intensity. Uninjected larvae (open squares), larvae injected with control MO (closed squares), 40 ng ATG Mo (closed circles) and 16 ng GT Mo (triangles) were analyzed. Averaged data are plotted with error bars showing mean±s.e.m. (D) RT-PCR analysis of aberrant splicing of *pcdh15b* transcript. The upper gel contains products amplified with primers flanking exon 4. The lower band is the predicted product without exon 4. The uppermost band presumably includes an extra intronic sequence. The lower gel shows a control reaction with *elongation factor* –1alpha. Lane 1, GT Mo-injected larvae, day 3; lane 2, uninjected larvae, day 3; lane 3, GT Mo-injected larvae, day 4, lane 4, uninjected larvae, day 5 (pool of 5 larvae per lane). Representative examples of ERG records from four different specimens under dark-adapted (E) and light-adapted states (F). Each trace is an average of 3-7 consecutive responses. Stimulus duration was 100 mseconds. Attenuated light intensity was presented as OD (optical density unit).

2001; Alagramam et al., 2001b), is duplicated in zebrafish. In larvae, Pcdh15a is specifically required in the ear, whereas Pcdh15b is required in the developing eye. The expression patterns of the two *pcdh15* paralogs provides insight into the evolution of these two genes. After gene duplication, one of the paralogous genes is often lost from the genome due to its redundant function (Prince and Pickett, 2002). If duplicated genes acquire non-redundant functions, then both are likely to be retained (Force et al., 1999). In the case of the *pcdh15* zebrafish paralogues, the high divergence of the intracellular domains may account for an adaptation or specialization of function of these two genes in the eye and ear. Although *pcdh15a* and *pcdh15b* are required in different sensory organs, both *pcdh15* genes retained a function in maintaining the structural integrity of the specialized apical surfaces of the respective sensory receptor cells.

In a recent study, PCDH15 protein was shown to be localized at the stereociliary bundle of hair cells in mammals (Ahmed et al., 2003a). This result is consistent with the bundle phenotype we detected in *orbiter* mutants, suggesting that *orbiter/pcdh15a* encodes a component of the stereociliary bundle. The large extracellular domain of Pcdh15a, along with the localization data from mammals, suggests that Pcdh15a may be part of the outer membrane calyx or a component of the extracellular links spanning neighboring stereocilia. Although the bundle phenotype is mild in *orbiter* mutants, microphonic potentials are not detectable in larvae carrying the strong allele. This phenotype raises the possibility that Pcdh15a plays a functional role in hair bundles.

In the *pcdh15b* morphants, the tilted outer segment phenotype suggests at least two possible functions of *pcdh15b* during differentiation. First, Pcdh15b may be necessary for adhesive contact between the outer segment of photoreceptors and the retinal pigment epithelium. Interestingly, when the retinal pigment epithelium is absent in the zebrafish retina, the outer segments are tilted sideways in a similar way (C. Seiler and A. Rojas-Munoz, unpublished). This phenotype suggests that the outer segments are actively intercalated into the pigmented epithelium. This paradigm requires *trans* interactions of at least two cadherins expressed in photoreceptors and the retinal pigment epithelium, but we could not detect *pcdh15b* in the pigment epithelium. Another possibility is that Pcdh15b is required for stabilization of photoreceptor outer segments. Such contacts may help to align the outer segments, making interdigitation with the retinal pigment epithelium possible. The localization pattern of PCDH15 in photoreceptor outer segments in the human and monkey retina (Ahmed et al., 2003a) appears to be consistent with these notions. PCDH15 protein was also detected in other layers of the fetal and adult human retina, especially the synaptic layers, and may play a role in synaptogenesis as well (Alagramam et al., 2001b).

To date, the only mouse mutant in an Usher gene reported to have a morphological defect in the eye is the *shaker1/Myo7a*

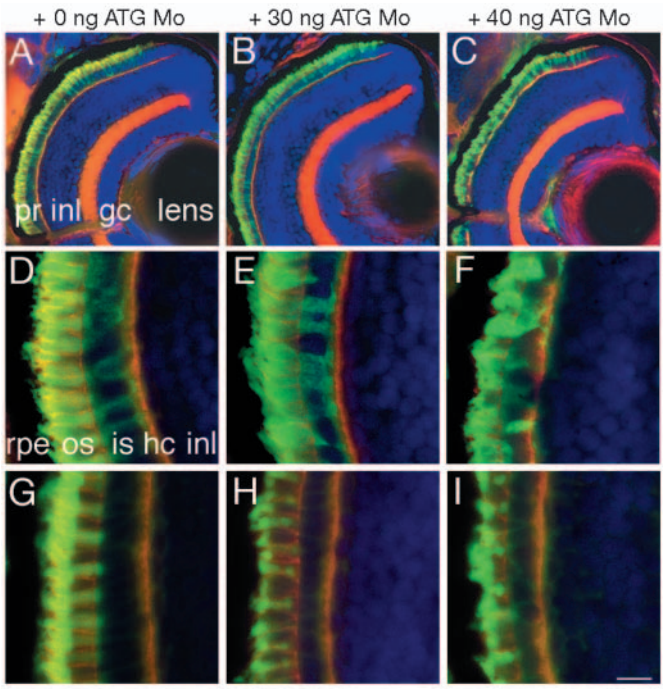

Fig. 6. Knock-down of *pcdh15b* function shows a dose-dependent effect on photoreceptor structure. (A-I) Cryosections of the proximal region of day 4 retinas were stained with Alexa568-Phalloidin (red), and DAPI (blue). All layers are present in the ATG Mo-injected larvae (B,C). The outer segments of rod photoreceptors were stained with zpr-1 antibody (A-F, green) or double cone photoreceptors were stained with rhod-1 antibody (G-I, green). Uninjected larvae (A,D,G), larvae injected with 30 ng ATG Mo (B,E,H), and larvae injected with 40 ng ATG Mo (C,F,I) are shown. Double cone receptors are disorganized and broader in appearance (E,F), and rod outer segments appear shorter and clumped together (H,I). Scale bar in I, 20 μm for A-C; and 5 μm for D-I. gc, ganglion cells; hc, horizontal cells; inl, inner nuclear layer; is, inner segments; os, outer segments; pr, photoreceptors; rpe, retinal pigment epithelium.

mutant. In *shaker1* mutants, the melanosomes of the retinal pigment epithelium do not migrate between photoreceptors, suggesting that myosin VIIA is needed for transport of these pigmented structures into the apical processes of retinal pigment cells (Liu et al., 1998). Slight reductions in ERG responses have also been detected in myosin VIIA mutant mice (Libby and Steel, 2001). Moreover, myosin VIIA has been shown to be expressed and required in the retinal pigment epithelium for uptake of outer segment disks (Gibbs et al., 2003). These results suggest that myosin VIIA also participates in photoreceptor and retinal pigment epithelium interactions.

In human Usher syndrome, retinitis pigmentosa develops in the second to third decade of life. This late defect in humans contrasts with the very early onset of photoreceptor malformation in zebrafish *pcdh15b* morphants. It is worth noting that in zebrafish, the eye develops much faster than in mammals (O'Brien et al., 2003; Sharma et al., 2003). Within 2.5 days, the zebrafish eye develops from a undifferentiated neuroephithelium to a layered and differentiated functional organ (Easter and Malicki, 2002). Furthermore, a fully populated photoreceptor cell layer develops within 30 hours (Raymond et al., 1995).

Thus, the contact and migration of outer segments into the retinal pigment epithelium happens much faster in zebrafish, and proper function of Pcdh15 appears critical at this timepoint. In various mouse models for retinal degeneration, the photoreceptor cell layer is initially disorganized and shows severe degeneration later in life [for example *rd8*/*Crb1* (Mehalow et al., 2003) *rd6*/*Mfrp* (Hawes et al., 2000; Kameya et al., 2002)]. Due to the limited efficiency of antisense morpholinos, we were not able to investigate juvenile stages to look for degeneration. However, photoreceptor interactions with the retinal pigment epithelium have been shown to be important for the outer segment disc phagocytosis, visual pigment renewal, and nutrient supply (Boulton and Dayhaw-Barker, 2001; Pacione et al., 2003). Moreover, progressive death of photoreceptors was observed in the vitiligo/*Mitf* mouse mutant in which retinal pigment epithelium initially failed to interdigitate with photoreceptors (Sidman et al., 1996), and in mutant *vestigial outer segments* zebrafish, which exhibit a similar phenotype to *pcdh15b* morphants (Manzoor-Ali et al., 2003). Thus, impaired contact between the retina pigment epithelium and the outer segments may cause degeneration at later stages.

The phenotypes observed in either mutant *orbiter*/*pcdh15a* zebrafish or *pcdh15b* morphants indicate a clear requirement for Pcdh15 proteins in hearing and vision in zebrafish. The sensory receptors in either the ear or the eye rely upon these protocadherins for structural integrity. Our study establishes a

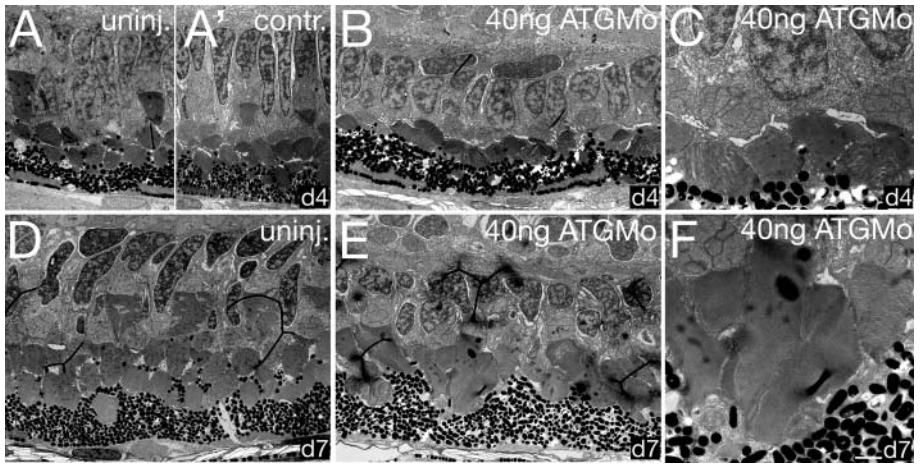

Fig. 7. Photoreceptor outer segments are tilted and clumped in *pcdh15b* morphants. Electron micrographs of day 4 (A-C) and day 7 (D-F) retinas of uninjected or 40 ng *pcdh15b* ATG Mo-injected larvae. The outer segments are slanted sideways and the nuclear layer is more condensed in morphants (B) in comparison to segments in uninjected larvae (A) or control 4 bp mismatch Mo-injected larvae (A′). In *pcdh15b* morphants, pigments cell melanosomes are rarely present between photoreceptor outer segments (B,D). The phenotype does not recover at day 7 and outer segments are often clustered together (D). (C,F) Higher magnification views of (B) and (E). Scale bar in F: 1 μm for A,B,D,E; 350 nm for C,F.

role for Pcdh15 in maintaining the structural integrity of the photoreceptor outer segment, and highlights the usefulness of an alternative animal model in studying the function of Usher genes.

We are grateful to the Sanger Institute for sequencing our contig clones. We thank Brigitte Sailer for her technical assistance with the TEM analysis. We would also like to thank P. Mayinger, R. Walker, and S. Jesusthasan for helpful comments on the manuscript.

Supplementary material

Supplementary material for this article is available at
http://dev.biologists.org/cgi/content/full/132/3/615/DC1

References

Ahmed, Z. M., Riazuddin, S., Bernstein, S. L., Ahmed, Z., Khan, S., Griffith, A. J., Morell, R. J., Friedman, T. B. and Wilcox, E. R. (2001). Mutations of the protocadherin gene PCDH15 cause Usher syndrome type 1F. *Am. J. Hum. Genet.* **69**, 25-34.

Ahmed, Z. M., Riazuddin, S., Ahmad, J., Bernstein, S. L., Guo, Y., Sabir, M. F., Sieving, P., Griffith, A. J., Friedman, T. B., Belyantseva, I. A. et al. (2003a). PCDH15 is expressed in the neurosensory epithelium of the eye and ear and mutant alleles are responsible for both USH1F and DFNB23. *Hum. Mol. Genet.* **12**, 3215-3223.

Ahmed, Z. M., Riazuddin, S. and Wilcox, E. R. (2003b). The molecular genetics of Usher syndrome. *Clin. Genet.* **63**, 431-444.

Alagramam, K. N., Murcia, C. L., Kwon, H. Y., Pawlowski, K. S., Wright, C. G. and Woychik, R. P. (2001a). The mouse Ames waltzer hearing-loss mutant is caused by mutation of Pcdh15, a novel protocadherin gene. *Nat. Genet.* **27**, 99-102.

Alagramam, K. N., Yuan, H., Kuehn, M. H., Murcia, C. L., Wayne, S., Srisailpathy, C. R., Lowry, R. B., Knaus, R., van Laer, L., Bernier, F. P. et al. (2001b). Mutations in the novel protocadherin PCDH15 cause Usher syndrome type 1F. *Hum. Mol. Genet.* **10**, 1709-1718.

Ball, S. L., Bardenstein, D. and Alagramam, K. N. (2003). Assessment of retinal structure and function in Ames waltzer mice. *Invest. Ophthalmol. Vis. Sci.* **44**, 3986-3992.

Ben-Yosef, T., Ness, S. L., Madeo, A. C., Bar-Lev, A., Wolfman, J. H., Ahmed, Z. M., Desnick, R. J., Willner, J. P., Avraham, K. B., Ostrer, H. et al. (2003). A mutation of PCDH15 among Ashkenazi Jews with the type 1 Usher syndrome. *N. Engl. J. Med.* **348**, 1664-1670.

Boulton, M. and Dayhaw-Barker, P. (2001). The role of the retinal pigment epithelium: topographical variation and ageing changes. *Eye* **15**, 384-389.

Easter, S. S., Jr and Malicki, J. J. (2002). The zebrafish eye: developmental and genetic analysis. *Results Probl. Cell Differ.* **40**, 346-370.

Force, A., Lynch, M., Pickett, F. B., Amores, A., Yan, Y. L. and Postlethwait, J. (1999). Preservation of duplicate genes by complementary, degenerative mutations. *Genetics* **151**, 1531-1545.

Geisler, R., Rauch, G. J., Baier, H., van Bebber, F., Brobeta, L., Dekens, M. P., Finger, K., Fricke, C., Gates, M. A., Geiger, H. et al. (1999). A radiation hybrid map of the zebrafish genome. *Nat. Genet.* **23**, 86-89.

Gibbs, D., Kitamoto, J. and Williams, D. S. (2003). Abnormal phagocytosis by retinal pigmented epithelium that lacks myosin VIIa, the Usher syndrome 1B protein. *Proc. Natl. Acad. Sci. USA* **100**, 6481-6486.

Granato, M., van Eeden, F. J., Schach, U., Trowe, T., Brand, M., Furutani-Seiki, M., Haffter, P., Hammerschmidt, M., Heisenberg, C. P., Jiang, Y. J. et al. (1996). Genes controlling and mediating locomotion behavior of the zebrafish embryo and larva. *Development* **123**, 399-413.

Haffter, P., Granato, M., Brand, M., Mullins, M. C., Hammerschmidt, M., Kane, D. A., Odenthal, J., van Eeden, F. J., Jiang, Y. J., Heisenberg, C. P. et al. (1996). The identification of genes with unique and essential functions in the development of the zebrafish, Danio rerio. *Development* **123**, 1-36.

Hawes, N. L., Chang, B., Hageman, G. S., Nusinowitz, S., Nishina, P. M., Schneider, B. S., Smith, R. S., Roderick, T. H., Davisson, M. T. and Heckenlively, J. R. (2000). Retinal degeneration 6 (rd6): a new mouse model for human retinitis punctata albescens. *Invest. Ophthalmol. Vis. Sci.* **41**, 3149-3157.

Hudspeth, A. J. (1989). How the ear's works work. *Nature* **341**, 397-404.

Kameya, S., Hawes, N. L., Chang, B., Heckenlively, J. R., Naggert, J. K. and Nishina, P. M. (2002). Mfrp, a gene encoding a frizzled related protein, is mutated in the mouse retinal degeneration 6. *Hum. Mol. Genet.* **11**, 1879-1886.

Larison, K. D. and Bremiller, R. (1990). Early onset of phenotype and cell patterning in the embryonic zebrafish retina. *Development* **109**, 567-576.

Libby, R. T. and Steel, K. P. (2001). Electroretinographic anomalies in mice with mutations in Myo7a, the gene involved in human Usher syndrome type 1B. *Invest. Ophthalmol. Vis. Sci.* **42**, 770-778.

Libby, R. T., Kitamoto, J., Holme, R. H., Williams, D. S. and Steel, K. P. (2003). Cdh23 mutations in the mouse are associated with retinal dysfunction but not retinal degeneration. *Exp. Eye Res.* **77**, 731-739.

Liu, X., Ondek, B. and Williams, D. S. (1998). Mutant myosin VIIa causes defective melanosome distribution in the RPE of shaker-1 mice. *Nat. Genet.* **19**, 117-118.

Makhankov, Y. V., Rinner, O. and Neuhauss, S. (2004). An inexpensive device for non-invasive electroretinography in small aquatic vertebrates. *J. Neurosci. Methods* **135**, 205-210.

Manley, G. A. and Koppl, C. (1998). Phylogenetic development of the cochlea and its innervation. *Curr. Opin. Neurobiol.* **8**, 468-474.

Manzoor-Ali, P., Beckwith, L., Gladys, S., Moore, J., Wong, A., Chinoy, M. and Cheng, K. (2003). Histology-based screen for zebrafish mutants with abnormal cell differentiation. *Dev. Dyn.* **228**, 414-423.

Mehalow, A. K., Kameya, S., Smith, R. S., Hawes, N. L., Denegre, J. M., Young, J. A., Bechtold, L., Haider, N. B., Tepass, U., Heckenlively, J. R. et al. (2003). CRB1 is essential for external limiting membrane integrity and photoreceptor morphogenesis in the mammalian retina. *Hum. Mol. Genet.* **12**, 2179-2189.

Nasevicius, A. and Ekker, S. C. (2000). Effective targeted gene 'knockdown' in zebrafish. *Nat. Genet.* **26**, 216-220.

Nicolson, T., Rusch, A., Friedrich, R. W., Granato, M., Ruppersberg, J. P. and Nusslein-Volhard, C. (1998). Genetic analysis of vertebrate sensory hair cell mechanosensation: the zebrafish circler mutants. *Neuron* **20**, 271-283.

O'Brien, K. M., Schulte, D. and Hendrickson, A. E. (2003). Expression of photoreceptor-associated molecules during human fetal eye development. *Mol. Vis.* **9**, 401-409.

Pacione, L. R., Szego, M. J., Ikeda, S., Nishina, P. M. and McInnes, R. R. (2003). Progress toward understanding the genetic and biochemical mechanisms of inherited photoreceptor degenerations. *Annu. Rev. Neurosci.* **26**, 657-700.

Petit, C. (2001). Usher syndrome: from genetics to pathogenesis. *Annu. Rev. Genomics Hum. Genet.* **2**, 271-297.

Popper, A. N. and Fay, R. R. (1997). Evolution of the ear and hearing: issues and questions. *Brain Behav. Evol.* **50**, 213-221.

Popper, A., Platt, C., Webster, D. B., Fay, R. R. and Popper, A. N. (1992). Evolution of the vertebrate ear: an overview of ideas In *The Evolutionary biology of hearing*. New York, NY: Springer-Verlag.

Prince, V. E. and Pickett, F. B. (2002). Splitting pairs: the diverging fates of duplicated genes. *Nat. Rev. Genet.* **3**, 827-837.

Raphael, Y., Kobayashi, K. N., Dootz, G. A., Beyer, L. A., Dolan, D. F. and Burmeister, M. (2001). Severe vestibular and auditory impairment in three alleles of Ames waltzer (av) mice. *Hear Res.* **151**, 237-249.

Raymond, P. A., Barthel, L. K. and Curran, G. A. (1995). Developmental patterning of rod and cone photoreceptors in embryonic zebrafish. *J. Comp. Neurol.* **359**, 537-550.

Schulte-Merker, S., Hammerschmidt, M., Beuchle, D., Cho, K. W., de Robertis, E. M. and Nusslein-Volhard, C. (1994). Expression of zebrafish goosecoid and no tail gene products in wild-type and mutant no tail embryos. *Development* **120**, 843-852.

Seiler, C. and Nicolson, T. (1999). Defective calmodulin-dependent rapid apical endocytosis in zebrafish sensory hair cell mutants. *J. Neurobiol.* **41**, 424-434.

Sharma, R. K., O'Leary, T. E., Fields, C. M. and Johnson, D. A. (2003). Development of the outer retina in the mouse. *Brain Res. Dev. Brain Res.* **145**, 93-105.

Sheng, M. and Sala, C. (2001). PDZ domains and the organization of supramolecular complexes. *Annu. Rev. Neurosci.* **24**, 1-29.

Sidman, R., Kosaras, B. and Tang, M. (1996). Pigment epithelium and retinal phenotypes in the vitiligo, mivit, mutant mouse. *Invest. Opthalmol. Vis. Sci.* **37**, 1097-1115.

Steel, K. P. and Kros, C. J. (2001). A genetic approach to understanding auditory function. *Nat. Genet.* **27**, 143-149.

Taylor, J. S., Braasch, I., Frickey, T., Meyer, A. and van de Peer, Y. (2003). Genome duplication, a trait shared by 22000 species of ray-finned fish. *Genome Res.* **13**, 382-390.